scientific reports

Check for updates

OPEN

Tuning TCR complex recruitment to the T cell antigen coupler (TAC) enhances TAC-T cell function

Trevor M. Morey[1], Tania Benatar[2], Stacey X. Xu[2], Ling Wang[2], Philbert Ip[2], Thanyashanthi Nitya-Nootan[2], Gargi Thakor[2], Andreas G. Bader[2], Christopher W. Helsen[2]✉ & Walid A. Houry[1,3]✉

The T cell antigen coupler (TAC) receptor is a novel synthetic receptor designed to maximize the therapeutic potential of T cells in the absence of tonic signaling or receptor-related toxicities. Prior studies indicated that TACs provide safe and long-lasting anti-tumor immunity in multiple preclinical models of solid tumors supported by mounting clinical evidence. TAC receptors function by targeting a cancer associated surface antigen while recapitulating natural T cell receptor (TCR) signaling, which involves both TCR/CD3 recruitment and intracellular CD4 co-receptor activity. While other receptor designs exist that redirect TCR signaling towards cancer associated antigens, the TAC technology is unique in that antigen binding is distinctly separated from TCR/CD3 complex recruitment. In the present study, we show that single amino-acid changes in the TAC domain responsible for TCR recruitment of a Claudin 18.2-directed TAC receptor led to enhanced in vivo functionality. Analyzing biophysical properties of the receptor suggests that TAC receptors with high TCR affinities are suboptimal compared to receptor constructs that show lower TCR affinities with notably fast off-rates. This work demonstrates that balancing TCR recruitment is critical when designing effective TAC T cell receptors, a concept that may apply more broadly to other therapeutic approaches relying on TCR signaling.

Keywords T cell therapy, T cell receptor (TCR), T cell antigen coupler (TAC), UCHT1, Cancer, Binding affinity, scFv

Treatment of cancer with adoptive cell therapies has garnered substantial interest in recent years due to the clinical success of engineered chimeric antigen receptor (CAR) T cells therapies. Briefly, autologous CAR-T therapies involve ex vivo engineering of patient T cells to express a synthetic receptor that recognizes tumor-specific antigens, thus enabling specific targeting of these engineered T cells to cancer cells[1]. While existing FDA-approved CAR-T therapies have shown clinical success towards hematological cancers, such as for B-cell non-Hodgkin lymphoma (NHL) or acute lymphoblastic leukemia (ALL), these approaches have failed to show efficacy against solid tumors[2,3]. Moreover, CAR-T therapies frequently elicit serious side effects, including cytokine release syndrome and neurological toxicities[4,5], and CARs have been shown to have substantially lower antigen sensitivity compared to native T cell receptors (TCRs), making CARs unsuitable for targeting cancer antigens with low expression levels[6]. To overcome these limitations, recent improvements in T cell engineering have refocused on methods whereby the engineered receptors engage with and utilize endogenous TCRs rather than, as in the case with CAR-T therapies, bypassing the TCR complex. One such example includes the HLA-independent TCR (HIT) and synthetic TCR and antigen receptor (STAR), which exchange the variable domains of the TCR with a tumor-antigen binder in an HLA-independent manner[7,8]. Other approaches include the T cell receptor fusion construct (TRuC) that covalently links the antigen-binder to CD3ε[9], and the T cell antigen coupler (TAC)[10], which is described below.

The TAC receptor (Fig. 1A) contains three functional domains: (1) a targeted, though interchangeable extracellular antigen recognition domain, such as a nanobody specific for Claudin (CLDN)-18.2, (2) a TCR-binding domain, typically an anti-CD3ε single-chain variable fragment (scFv) such as UCHT1[11] (Figs. 1A,B and S1), that allows for engagement of TAC receptors with the endogenous TCR complex, and (3) a CD4 co-receptor

[1]Department of Biochemistry, University of Toronto, 661 University Avenue, MaRS Centre, West Tower, Room 1612, Toronto, ON M5G 1M1, Canada. [2]Triumvira Immunologics Inc, 270 Longwood Road South, Hamilton, ON L8P 0A6, Canada. [3]Department of Chemistry, University of Toronto, Toronto, ON M5S 3H6, Canada. ✉email: cwhelsen@triumvira.com; walid.houry@utoronto.ca

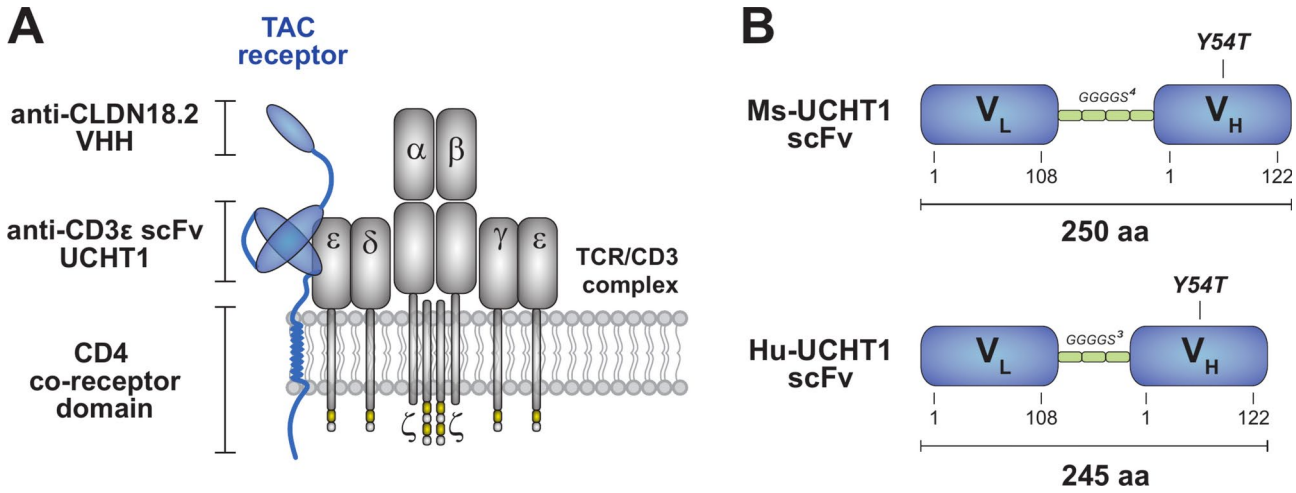

Fig. 1. Overview of the T cell antigen coupler (TAC) receptor and UCHT1 scFv. (**A**) Shown is the TAC receptor mechanism-of-action. The TAC receptor (blue) recruits the endogenous T cell receptor (TCR; grey) complex through binding of the UCHT1 scFv domain to CD3ε. Antigen is bound separately via the antigen recruitment domain, for example a CLDN18.2-targeting single chain nanobody (VHH). The TAC receptor is anchored into the plasma membrane using the CD4 co-receptor domain (intracellular, transmembrane, and extracellular flexible loop). (**B**) The murine (Ms) and humanized (Hu) UCHT1 scFvs are designed from and contain the UCHT1 light chain (V_L; amino acids 1-108) and heavy chain (V_H; amino acids 1-122) linked together with a flexible 4 × or 3 × GGGGS linker, respectively. Residue Tyr^{54}, which is mutated in this study (Y54T), is located within the UCHT1 heavy chain.

UCHT1 Variant	Species	Literature Observations	References
Ms-UCHT1 Wild-type (WT)	Murine (Ms)	Discovery of UCHT1 antibody Crystal structure of Ms-UCHT1 scFv bound to CD3εδ Critical to TAC receptor function Inferior in vivo potency to humanized variants	10, 11, 13, 19
Ms-UCHT1 Y54T	Murine (Ms)	Surface expression superior to Ms-WT UCHT1 In vivo potency superior to Ms-WT UCHT1	15
Hu-UCHT1 Wild-type (WT)	Humanized (Hu)	Humanization of UCHT1 antibody Critical to TAC receptor function Surface expression superior to Ms-WT UCHT1 In vitro binding to PBMCs enhanced vs. Ms-WT UCHT1	10, 13, 16, 17
Hu-UCHT1 Y54T	Humanized (Hu)	Surface expression superior to Ms- and Hu-WT UCHT1 In vitro binding to PBMCs enhanced vs. Ms-WT UCHT1 In vivo potency superior to Ms-WT UCHT1	13

Table 1. List of pre-existing studies on the TAC receptor with comparison of mutants within the CD3ε-binding UCHT1 scFv domain.

domain that anchors the TAC receptor to the plasma membrane and provides receptor functionality. Preclinical testing of human T cells engineered to express TAC receptors has shown that this technology is highly potent against antigen-positive liquid ($BCMA^+$ or $CD19^+$) and solid ($HER2^+$ or $CLDN18.2^+$) tumors, both in cells and using in vivo mouse models, without causing the side effects associated with CAR-T therapies[10,12,13]. Based on these preclinical results, this technology has been extended into phase 1/2 clinical trials where autologous T cells engineered to express CLDN18.2-targeted TAC receptors are being investigated as a novel treatment for unresectable, locally advanced, or metastatic $CLDN18.2^+$ solid tumors (TAC01-CLDN18.2; ClinicalTrials.gov: NCT05862324)[14].

A unique feature of the TAC technology is that TAC-mediated T cell activation is modulated synergistically by both the antigen-binding domain (e.g. anti-CLDN18.2) and by binding to the TCR complex through the CD3ε-binding UCHT1 scFv domain of the TAC receptor. This enables optimization of the TAC receptor by fine tuning TCR complex recruitment via the UCHT1 scFv domain without having to modify affinity towards the cell surface tumor antigen. Consequently, by mutagenesis of the prototypic murine (Ms) UCHT1 scFv heavy chain, we have previously identified a Y54T mutant that increased TAC receptor function (Table 1)[15]. Subsequent studies have investigated TAC receptors with a humanized (Hu) UCHT1 scFv domain[16] alongside a related Hu-Y54T variant, both of which increased the in vivo anti-tumor efficacy of these TAC receptors as compared to the original Ms-UCHT1 scFv domain (Table 1)[13]. While these studies, as well as observations made throughout the preclinical development of the TAC01-CLDN18.2 therapy[17], have repeatedly shown that changes to the CD3ε-binding UCHT1 scFv domain impact TAC receptor function[10,13,15], the mechanisms

resulting in these observations remain elusive. Therefore, as one potential factor contributing to these in vivo functional differences, the work presented here aimed to biochemically assess the direct interaction between multiple UCHT1 scFv variants to their substrate CD3ε. Altogether, we show that a weaker affinity between in vitro purified Hu-Y54T UCHT1 scFv and recombinant CD3εδ heterodimer correlates with increased in vivo efficacy of Hu-Y54T UCHT1-containing TAC receptors in CLDN18.2-expressing tumor mouse models. These results suggest a new affinity-based model by which future improved TAC receptors can be rationally designed and tested.

Results

In vivo testing of the Hu-Y54T UCHT1-CLDN18.2-TAC

The development of the CLDN18.2-TAC technology has been detailed in a prior study wherein we have shown that human T cells expressing CLDN18.2-TAC receptors induce a specific, potent, and long-lasting anti-tumor response in various CLDN18.2-expressing cellular and in vivo solid tumor models while being well tolerated and showing no TAC related toxicities[17]. In addition to this work, and as part of the continued preclinical development of the TAC01-CLDN18.2 therapy (ClinicalTrials.gov: NCT05862324), an ideal TAC receptor design had to be identified. Previously, variants of the CD3ε-binding UCHT1 scFv domain have been shown to affect the performance of HER2- and BCMA-targeted TAC receptors in cellular and in vivo studies, with humanized variants demonstrating the greatest anti-tumor potency (Table 1). Thus, we generated anti-CLDN18.2 TAC variants containing either a wild-type (WT) humanized (Hu) UCHT1 or mutant Hu-Y54T UCHT1 scFv domain and, subsequently, evaluated both in cells and in vivo (Fig. 2). As measured by flow cytometry, when expressed in human primary T cells, the Hu-Y54T TAC variant showed enhanced TAC receptor surface expression as compared to the wild-type variant (Fig. 2A). Furthermore, when co-cultured with CLDN18.2$^+$ KATO III cells, surface expression of CD69, a marker of early T cell activation[18], was higher in CD8$^+$ mature cytotoxic T cells upon expression of the Hu-Y54T TAC variant compared to wild-type (Fig. 2B), indicative of a stronger T cell activation.

For in vivo evaluation using adoptive cell therapy (ACT), immune-deficient NSG mice were first inoculated with NALM6$^{eLuc/CLDN18.2}$ liquid B-cell acute lymphoblastic tumors (i.v.), or with either NCI-N87$^{CLDN18.2}$ or CLDN18.2$^+$ OE19 gastric/esophageal solid tumors (s.c.), then treated with TAC-engineered human T cells expressing either the Hu-WT or mutant Hu-Y54T UCHT1-CLDN18.2-TAC. When tumor-bearing mice were treated with higher dose levels of Hu-WT UCHT1-CLDN18.2 TAC-engineered T cells (4.0×10^6–1.2×10^7 cells) full attenuation of NALM6 tumor growth was observed compared to control non-transduced T cells (Fig. 2C). Additionally, expression of either Hu-WT or Hu-Y54T UCHT1-CLDN18.2-TAC led to tumor regression in both NCI-N87 and OE19 solid tumors following treatment with 6.0×10^6 TAC-engineered T cells (Figs. 2D and S2). While the Hu-WT and Hu-Y54T TAC variants appear to be equally effective in vivo at these dose levels, subsequent evaluation at lower dose levels (1.0×10^6 cells) revealed clear differences in their in vivo efficacy. Specifically, mice harboring either liquid NALM6 (Fig. 2E,F) or solid OE19 (Fig. 2G,H) tumors showed reduced tumor burden and increased survival when treated with engineered T cells expressing the Hu-Y54T UCHT1-CLDN18.2-TAC variant as compared to those treated with the Hu-WT UCHT1 TAC variant or control non-transduced cells. Furthermore, while the Hu-WT TAC variant failed to improve survivability in mice inoculated with NALM6 liquid tumors at this lower dose level (Fig. 2F), treatment of mice bearing OE19 solid tumors with Hu-WT TAC-expressing T cells increased survival as compared to those treated with control non-transduced cells (Fig. 2H). Overall, these results demonstrate the superior in vivo efficacy of the mutant Hu-Y54T TAC variant over the Hu-WT UCHT1-CLDN18.2-TAC.

Assessing the interaction between UCHT1 variants and CD3εδ

Next, we aimed to elucidate whether biophysical principles could underly the enhanced in vivo efficacy of the Hu-Y54T UCHT1-CLDN18.2-TAC variant. The crystal structure of the prototypic murine (Ms) UCHT1 scFv bound to a recombinant CD3εδ heterodimer has been previously solved[19]. Based on structural analysis (Fig. S3), it is reasonable to predict that the mutation of residue Tyr^{54} from an aromatic hydrophobic tyrosine to a neutral polar threonine could affect affinity and/or binding kinetics between the CLDN18.2-TAC and CD3ε of the TCR complex. To assess this interaction directly, we used recombinant UCHT1 scFv protein purified from *Escherichia coli*. While the UCHT1 scFv has been purified from *E. coli* previously, this has historically required denaturation and refolding of insoluble UCHT1 from inclusion bodies[13,19]. Thus, we developed an improved purification strategy to produce natively folded, soluble, and monomeric UCHT1 scFvs using the autoinduction expression system in *E. coli* cells[20]. Briefly, we expressed UCHT1 as a fusion protein containing an N-terminal periplasm-targeting pelB leader sequence, Myc-tagged UCHT1 scFv, TEV protease cleavage site, flexible GSSG^2 linker, and a C-terminal poly-His^8 tail (Fig. 3A). This fusion protein was then purified sequentially by Ni-NTA affinity purification, TEV protease cleavage to remove the poly-His^8 tag, and anion exchange chromatography (Fig. S4). For this study the following protein constructs were purified: **(1)** the Hu-WT UCHT1 scFv and **(2)** mutant Hu-Y54T variant, as well as **(3)** the prototypic Ms-WT UCHT1 scFv and **(4)** related Ms-Y54T mutant. Importantly, we were able to successfully purify these UCHT1 scFv variants from the soluble bacterial lysate without the need for a denaturing lysis or refolding. The overall purity of each UCHT1 preparation was ≥ 99%, and each protein migrated at the expected molecular weight of 28.5 kDa when run on SDS-PAGE gels (Figs. 3B and S5).

The in vitro stability and oligomeric status of each purified UCHT1 scFv was subsequently assessed by performing thermal denaturation assays over a 35–95 °C range using a Tycho NT.6 system or by size-exclusion chromatography (SEC), respectively. Overall, all variants were thermally stable, though both humanized UCHT1 scFvs had higher thermal stability (~ 86 to 87 °C) compared to either of the Ms-UCHT1 variants (~ 82 °C; Fig. 3C and Table 2). No difference was observed for either the murine or humanized UCHT1 scFvs when comparing the wild-type to mutant Y54T, suggesting this mutation does not alter the thermal stability of the UCHT1 scFvs.

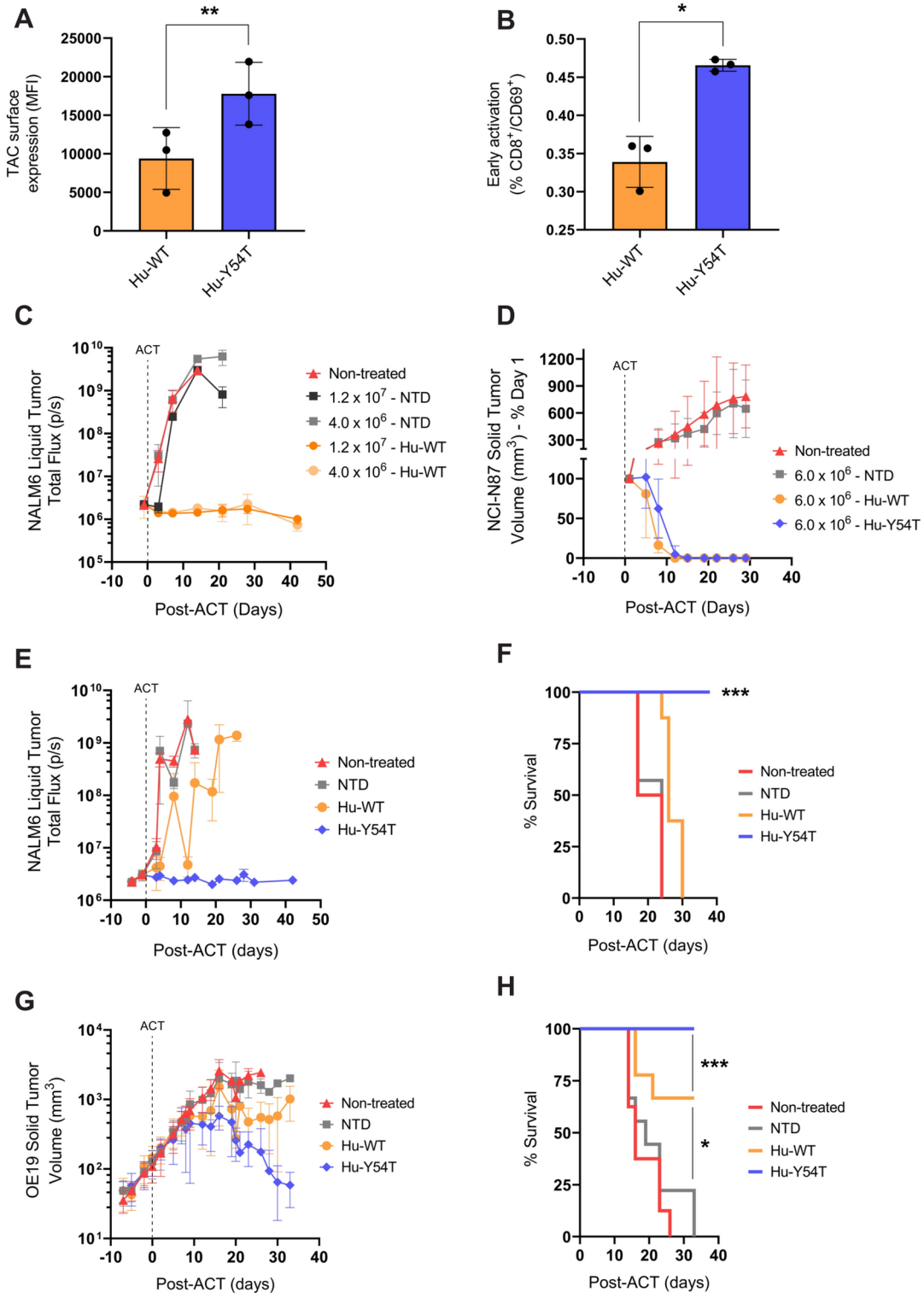

Importantly, SEC confirmed that the purified UCHT1 scFvs were monomeric and eluted from the column at the anticipated molecular weight (Figs. 3D-G and S6). Interestingly, during the purification of the Hu-WT and Hu-Y54T UCHT1 scFvs, we noted that these proteins eluted off the anion exchange column in multiple distinct peaks over a 50–600 mM NaCl gradient (Fig. S4C-D). When run on non-reducing Native-PAGE gels (Fig. S7A), the peaks eluting at low salt (~150 mM) appeared to contain a single monomeric species, whereas the peaks eluting at high salt (≥230 mM) contained a heterogenous population of higher molecular weight Hu-UCHT1 oligomers, a result that was confirmed using SEC (Fig. S7B,C). These findings are in line with previous work showing that scFvs can oligomerize[21,22], and that this can impact scFv binding affinities towards their targeted antigens[23]. Importantly, none of our purified UCHT1 scFvs were observed to elute in the void volume during SEC, indicating that all purifications were devoid of aggregated and/or insoluble proteins.

◀**Fig. 2**. In vivo anti-tumorigenic effects of the CLDN18.2-TAC. (**A, B**) Evaluation of cell-surface levels of TAC receptors (**A**) and early T cell activation (**B**; $CD8^+/CD69^+$) in transduced human primary T cells expressing Hu-WT UCHT1-CLDN18.2-TAC or mutant Hu-Y54T UCHT1-CLDN18.2-TAC that were co-cultured with $CLDN18.2^+$ KATO III cells. Data were collected by flow cytometry (Student's *t*-test, $^*p \le 0.05$, $^{**}p \le 0.01$; mean ± SD, $n = 3$). (**C**, **D**) Adoptive cell therapy (ACT) of NSG mice harboring $CLDN18.2^+$ liquid $NALM6^{eLuc/CLDN18.2}$ (**C**) or solid $NCI\text{-}N87^{CLDN18.2}$ (**D**) tumors treated with higher doses ($4.0–12.0 \times 10^6$ cells) of TAC-engineered T cells expressing either a Hu-WT or Hu-Y54T UCHT1-CLDN18.2-TAC variant. Control mice were treated with non-transduced (NTD) human T cells or left untreated (mean ± SD, $n = 5–6$ mice per treatment group). (**E–H**) NSG mice harboring liquid $NALM6^{eLuc/CLDN18.2}$ (**E, F**) or NRG mice with $CLDN18.2^+$ solid OE19 (**G, H**) tumors were treated with TAC-engineered T cells expressing either Hu-WT or mutant Hu-Y54T UCHT1-CLDN18.2-TAC at lower doses (1.0×10^6 cells). Control mice were treated with non-transduced human T cells or left untreated. Total flux for liquid tumors (**C, E**) or tumor volume (mm^3) for solid tumors (**D**, **G**) was measured as a function of time (days) post-ACT. Percent (%) survival in both the liquid $NALM6^{eLuc/CLDN18.2}$ (**F**) and solid OE19 (**H**) tumor models were measured and compared (logrank test; $^*p \le 0.05$, $^{***}p \le 0.001$; mean ± SD, $n = 6–9$ mice per treatment group).

We next performed biolayer interferometry (BLI) to determine binding kinetics of our purified, soluble, and monomeric UCHT1 scFvs towards a recombinant biotinylated CD3εδ heterodimer purified from human HEK293 cells (ACROBiosystems). Importantly, we observed clear differences in both association and disassociation rates when comparing these murine and humanized UCHT1 scFv variants (Fig. 4A). Affinity binding curves were fitted using nonlinear regression with global analysis, and binding kinetics were calculated (Table 3). When comparing binding affinities of the different variants to CD3εδ (K_d; Fig. 4B), the following order of affinities was observed: the prototypic wild-type Ms-UCHT1 scFv had the strongest affinity (0.25 ± 0.10 nM), followed by Ms-Y54T and Hu-WT (1.11 ± 0.29 nM and 1.81 ± 0.63 nM, respectively), and lastly Hu-Y54T with the weakest affinity (29.3 ± 4.0 nM). The association rates (k_{on}; Fig. 4C) reveal trends whereby both humanized variants have a slower association rate compared to the murine variants. Lastly, the dissociation rates (k_{off}; Fig. 4D) inversely correlated with the observed K_d's such that the variants with weaker affinities displayed faster dissociation rates. Collectively this data demonstrates discreet changes in the in vitro binding kinetics of these UCHT1 scFv variants to their substrate CD3εδ, with the mutant Hu-Y54T variant having the weakest affinity of the tested UCHT1 scFvs exhibiting a slower k_{on} and faster k_{off}.

Discussion

We and others have demonstrated previously that various UCHT1-TAC receptor variants have significantly different cellular and in vivo properties (Table 1). Generally, the prototypic Ms-WT UCHT1-TAC shows low cell surface receptor expression and lesser in vivo potency[13]. This can be overcome by introduction of the Y54T mutation into the Ms-UCHT1 scFv domain, which increases receptor surface expression and in vivo functionality[15]. In the present study CLDN18.2-TAC receptors containing a humanized Y54T-UCHT1 scFv domain similarly displayed significantly enhanced surface expression and in vivo potency relative to the Hu-WT UCHT1-TAC. For these TAC variants, the increase in in vivo potency appears to correlate with a lower in vitro affinity of the purified recombinant UCHT1 scFvs towards CD3εδ (i.e. the TCR complex). While this suggests an advantage of a lower affinity UCHT1-TAC receptor, future studies are required to identify the mechanism by which reduced TAC-TCR affinity leads to enhanced in vivo activity. We speculate that lower TAC-TCR affinity, namely a slower k_{on} and faster k_{off}, could have multiple consequences in situ, including higher TAC surface expression, an observation made in our primary T cell model expressing the Hu-Y54T UCHT1-CLDN18.2-TAC (Fig. 2A), and/or more dynamic TAC-T cell signaling and activation. It is currently unknown whether these properties of the CLDN18.2-TAC receptor, namely TCR binding and cell-surface levels, act alone or synergistically to enhance in vivo TAC activity. However, it is important to note that in a related study investigating a BCMA-targeted Hu-Y54T UCHT1-TAC receptor that T cells engineered with elevated TAC surface levels were equally efficacious as those with lower TAC receptor cell surface levels in both long-term cellular and in vivo assays, suggesting that surface expression may not significantly impact TAC T cell efficacy[13].

Prior work on the TAC technology has focused primarily on improving in vivo and preclinical outcomes of TAC-T cell therapies, and thus our study represents an important step towards understanding the biochemical basis of the TAC/TCR interaction. Our in vitro studies allowed us to directly assess the interaction between different UCHT1 scFv variants and CD3εδ, and thus the purification of natively folded and monomeric UCHT1 was critical to accurately measure and compare binding kinetics. While production of Fc-containing full-length antibodies and antibody fragments is typically accomplished in mammalian cells, often resulting in post-translational glycosylation of the Fc region for stability and activity[24,25], scFvs that lack an Fc region, have proven to be a class of antibody fragments suitable for expression in *E. coli*, which lack the N-glycosylation modification system present in eukaryotic cells[26]. Prior studies have purified UCHT1 scFvs from *E. coli* by refolding from insoluble inclusion bodies[13,19]. Protein refolding techniques can unintentionally disrupt native disulfide bonds and/or promote protein oligomerization in vitro, leading to production of soluble, yet oligomeric proteins with enhanced or altered binding affinities[23,27]. Of note, intramolecular disulfide bonds have been found important for the soluble expression, in vitro stability, and function of various scFvs[28–30], and the Ms-UCHT1 scFv contains two disulfide bonds between residues Cys^{22}-Cys^{96} and Cys^{24}-Cys^{89} on the UCHT1 heavy and light chains, respectively (Fig. S3)[19]. Importantly, and first to our knowledge, we have successfully purified soluble and monomeric UCHT1 scFvs from *E. coli* without the need for a denaturing/reducing lysis or refolding step. Interestingly, we found that the humanized UCHT1 scFvs had the capacity to form both monomers and higher

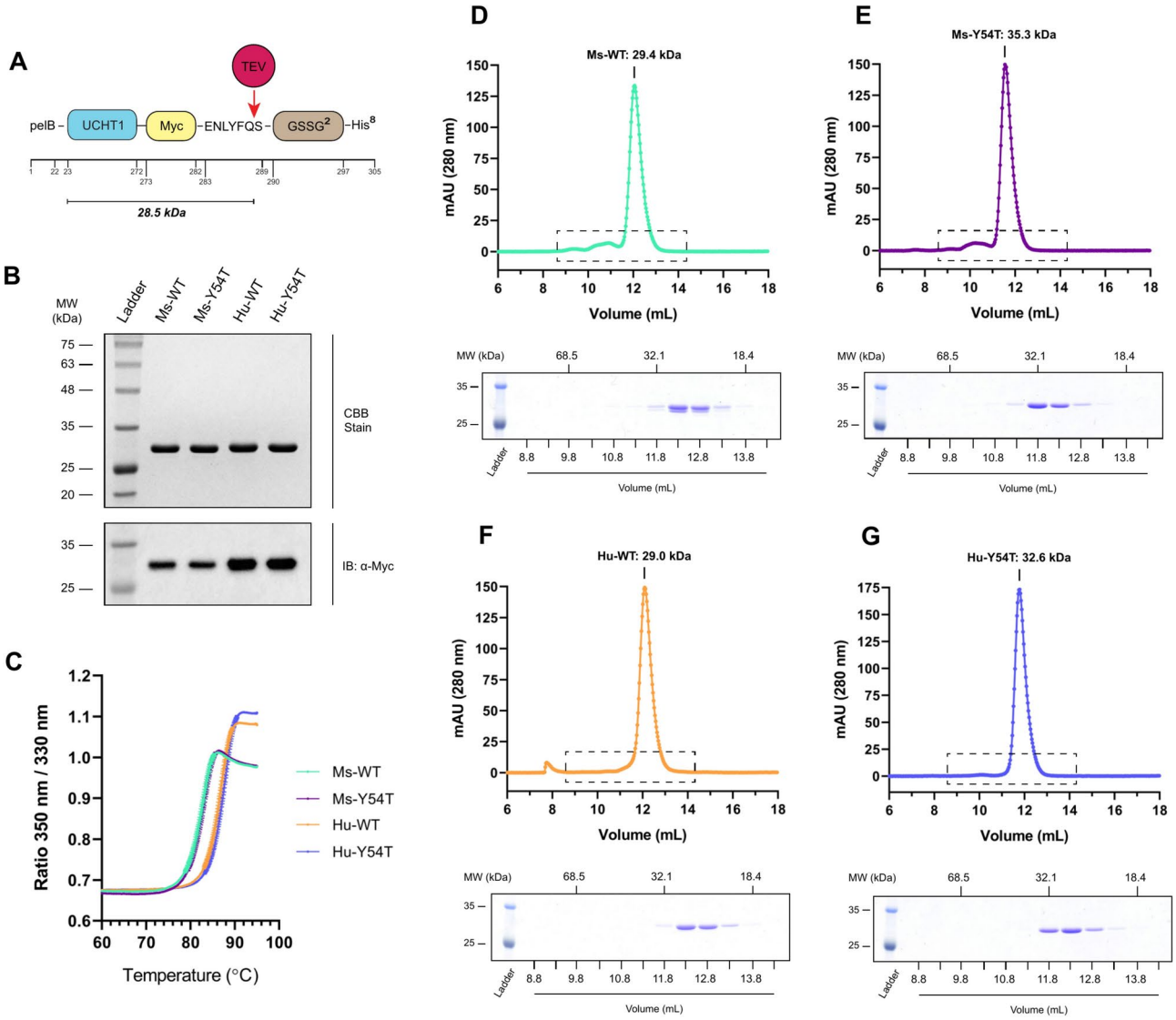

Fig. 3. In vitro purification and characterization of UCHT1 scFv variants from *E. coli*. (**A**) Recombinant UCHT1 scFv is expressed as a fusion protein containing a N-terminal periplasm-targeting pelB leader sequence, Myc-tagged UCHT1 scFv, TEV protease cleavage site, flexible $GSSG^2$ linker, and a C-terminal poly-His^8 tail. The final purified UCHT1-Myc scFv has an expected molecular weight of 28.5 kDa. Amino acid residue numbers (1-305) are shown with the final purified product containing amino acids 23-288. (**B**) Representative Coomassie Brilliant Blue (CBB)-stained SDS-PAGE gel and anti-Myc immunoblot (IB) loaded with purified Ms- or Hu-UCHT1-Myc variants. (**C**) Thermal shift assays of purified UCHT1 scFvs. Denaturation midpoint (T_m) was determined by tracking increased protein unfolding at 350 nm relative to folded protein at 330 nm over a 35–95 °C range (mean ± SD, $n = 4$). (**D**-**G**) Size exclusion chromatography profiles of purified UCHT1 scFvs. Ms-WT (**D**), Ms-Y54T (**E**), Hu-WT (**F**), and Hu-Y54T (**G**) scFvs were separated on a Superdex 75 Increase 10/300 GL column. Protein samples (hatched box) were run on SDS-PAGE gels and CBB-stained (panels under chromatogram). The elution of UCHT1 from the column was monitored at 280 nm and chromatographic traces for each UCHT1 variant were graphed with the estimated molecular weight shown for each peak ($n = 1$).

molecular weight soluble oligomers in vitro (Figs. S4 and S5). When comparing the monomeric Hu-UCHT1 scFvs to each other, the Hu-Y54T UCHT1 scFv variant displayed a lower affinity towards CD3εδ compared to the wild-type Hu-UCHT1 scFv (Fig. 4 and Table 3), a result that differed from a prior study using recombinant Hu-UCHT1 scFvs that were refolded from insoluble inclusion bodies[13]. In the context of the engineered TAC receptor, it is unlikely that the UCHT1 scFv domain oligomerizes in situ as TAC-expressing T cells show no signs of tonic signaling or autoactivation[10], both being expected if TAC receptors were to oligomerize and promote TCR complex aggregation, a phenomenon well-documented for CAR receptors[31].

One limitation of our study is that we exclusively used BLI to determine affinity values for our UCHT1 scFv variants towards CD3εδ. Multiple techniques exist to measure protein–protein interactions and their related in

UCHT1	T_m (°C)	R^2
Ms-WT	81.67 ± 0.03	0.994
Ms-Y54T	81.97 ± 0.03	0.995
Hu-WT	86.20 ± 0.02	0.997
Hu-Y54T	87.07 ± 0.02	0.997

Table 2. Denaturation midpoint (T_m) values for each purified UCHT1 scFv variant from Fig. 3C.

vitro affinities, including enzyme-linked immunosorbent assays (ELISAs), isothermal colorimetry (ITC), surface plasmon resonance (SPR), and microscale thermophoresis (MST), all of which differ in their sample preparation, assay conditions, and detection[32]. Of these, BLI is often chosen for its high-throughput nature, being able to measure multiple proteins in parallel in the same assay plate, whereas SPR has demonstrated increased sensitivity for measuring affinities between proteins and small molecules[33]. Comparative studies between BLI and SPR that have used the same analyte/ligand have yielded differing conclusions, with two studies demonstrating minimal differences[34,35], while another reported discrepancy in dissociation rates, though demonstrated that a rate order hierarchy between different analytes were well preserved between these two techniques[36]. Thus, while care should be taken when interpreting absolute affinity values obtained from these various techniques, both BLI and SPR appear equally efficacious when comparing similar analytes, such as in our study of UCHT1 scFv variants.

In summary, this study provides evidence for an affinity-mediated mechanism that could be responsible for enhanced in vivo TAC receptor efficacy. Our data aligns with other studies reporting that moderate-to-low affinity binding is preferred for T cell activation when using synthetic receptors[37,38], including one study investigating a bispecific T cell engager containing UCHT1 scFv variants[39], suggesting that optimal T cell activation may benefit from dynamic and lower affinity TCR recruitment over static signal integration. Thus, our study may serve as a guide for the future rational design of improved TAC receptors and the clinical use thereof, specifically through reduction of TAC-TCR affinity, though we hypothesize that the ideal affinity to maximize TAC efficacy in vivo may sit within a dynamic range whereby too much or too little TCR affinity may negatively impact TAC functionality. Interestingly, endogenous TCR-mediated signaling has been found to be both highly sensitive, recognizing low antigen levels, while also being able to elicit a potent T cell response, properties derived from low affinity TCR-major histocompatibility complex (MHC) interactions[40,41]. Comparing our results to existing research on the TCR mechanism-of-action we find that our results agree with general observations, specifically that TCRs evolved around an optimal activation affinity to ensure high specificity and efficacy[41–43], and while the effect of excessive antigen affinity for TCR receptors is complex[44], high antigen affinity can result in reduced receptor activity and T cell function[45]. Thus, the findings presented here may be more broadly applicable such that, in general, moderate TCR recruitment may promote dynamic and optimal TCR activity.

Methods

Cloning of expression plasmids and lentiviral production

The CLDN18.2-TAC receptor was based on a 3rd generation scaffold[12] with the antigen-targeting anti-CLDN18.2 nanobody sequence provided by Sanyou Biopharmaceuticals. Synthetic DNA fragments for the CLDN18.2-TAC and human CLDN18.2 were purchased from either GeneArt (Thermo) or Integrated DNA Technology (IDT). The TAC construct was initially cloned into a lentiviral pCDH-MSCV-MCS-IRES-GFP cloning and expression vector (#CD731B-1; System Bioscience). For T cell engineering, TAC constructs were cloned into either a user-designed custom lentiviral expression vector (Origene) or a lentiviral pCDH-CMV-MCS-EF1α-Neo/Hygro vector (#CD514B-1/CD515B-1; System Bioscience). All constructs were cloned by standard restriction digestion, ligation, and/or by Gibson assembly. Lentivirus used for T cell transduction was prepared in-house using the LV-MAX Lentiviral Production System (Thermo) with the LV-MAX Lentiviral Packaging Mix (Thermo) and using the above lentiviral expression vectors. For in vitro work, DNA encoding for murine (Ms) and humanized (Hu) UCHT1 scFv variants was codon-optimized for expression in *E. coli* (K12), and the genes were synthesized by Integrated DNA Technologies to contain, from N-to-C-terminal, a periplasm-targeting pelB leader sequence, UCHT1 scFv[16,46], Myc-tag, TEV protease cleavage site, flexible $GSSG^2$ linker, and poly-His^8 tag. For T7-inducible expression in *E. coli*, synthesized UCHT1 scFv DNA was cloned into p11 plasmid using NcoI/BamHI.

Cell culture and T cell engineering

The following human cell lines were purchased from ATCC: gastric carcinoma KATO III (#HTB-103) and NCI-N87 (#CRL-5822), and B-cell acute lymphoblastic NALM6 (#CRL-3273). Human gastric cardia/esophageal adenocarcinoma OE19 cells (#96071721; ECACC) were purchased from Sigma. CLDN18-overexpressing $NALM6^{eLuc/CLDN18.2}$ and $NCI\text{-}N87^{CLDN18.2}$ cells were generated by lentiviral transduction. Cell lines were cultured using Advanced RPMI 1640 (Gibco) with 5% Fetal Bovine Serum (ATCC), 1 × Glutamax (Gibco), and Penicillin/Streptomycin (Gibco). For production of CLDN18.2-TAC-expressing T cells, human primary $CD4^+/CD8^+$ T cells were first purified from donated leukapheresis product (Hemacare) using anti-CD4/CD8 MicroBeads (#130-045-101/102; Miltenyi), then infected with homemade lentiviruses prepared as described above. Transduced T cells were subsequently grown using the G-Rex system (Wilson Wolf) in Advanced RPMI 1640 (Gibco) supplemented with heat-inactivated FBS (Gibco), 1 × Glutamax (Gibco), HEPES (Stemcell), β-mercaptoethanol (Gibco), Penicillin/Streptomycin (Gibco), 100 IU IL2 (CellGenix), and 10 ng/ml IL7 (CellGenix). Successful transduction was assessed via flow cytometry prior to cellular assays or in vivo work.

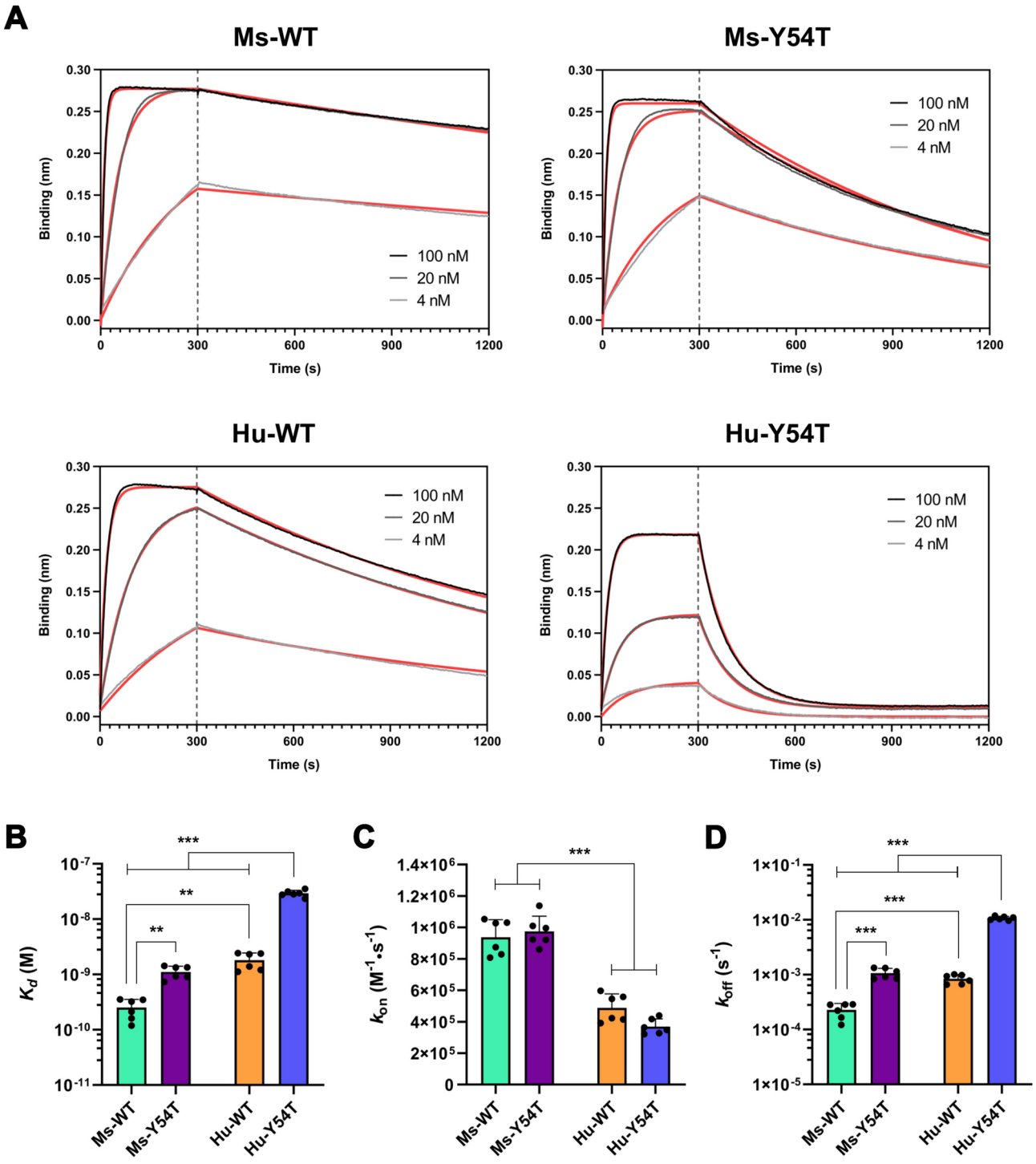

Fig. 4. Binding kinetic analysis of UCHT1 scFv variants. (**A**) Analysis of the binding of purified Ms- and Hu-UCHT1 scFv variants to CD3εδ using Bio-layer interferometry (BLI). Streptavidin-coated probes were loaded with biotinylated recombinant CD3εδ heterodimer (ACROBiosystems) and subsequently incubated independently with 100–4 nM of each UCHT1 scFv variant for 300 s. Dissociation rates were then measured over a 900 s period in kinetics buffer without UCHT1. Measurements were recorded using the Octet Red96 BLI system and analyzed using GraphPad Prism Software. Affinity binding curves (red) were fitted using nonlinear regression with global analysis. (**B**-**D**) Binding affinity (K_d; **B**), association rate (k_{on}; **C**), and dissociation rate (k_{off}; **D**) are graphed for each UCHT1 scFv variant for visual comparison. (Brown-Forsythe and Welch ANOVA with Dunnett's T3 post hoc test; $^{**}p \leq 0.01$, $^{***}p \leq 0.001$; mean ± SD, $n = 6$).

UCHT1	K_d (M)	k_{on} ($M^{-1}{\cdot}s^{-1}$)	k_{off} (s^{-1})	Global R^2
Ms-WT	$2.52 \pm 1.02 \times 10^{-10}$	$9.37 \pm 1.12 \times 10^{5}$	$2.28 \pm 0.71 \times 10^{-4}$	0.958
Ms-Y54T	$1.11 \pm 0.29 \times 10^{-9}$	$9.75 \pm 0.97 \times 10^{5}$	$1.07 \pm 0.23 \times 10^{-3}$	0.951
Hu-WT	$1.81 \pm 0.63 \times 10^{-9}$	$4.88 \pm 0.88 \times 10^{5}$	$8.39 \pm 1.58 \times 10^{-4}$	0.964
Hu-Y54T	$2.93 \pm 0.40 \times 10^{-8}$	$3.69 \pm 0.48 \times 10^{5}$	$1.07 \pm 0.08 \times 10^{-2}$	0.980

Table 3. Binding kinetic values for each purified UCHT1 scFv variant as calculated from Fig. 4A.

Cellular functional assays

For all functional assays, T cells were thawed one day prior and allowed to recover at 37 °C overnight. Prior to use, viable cells were counted using a Vi-CELL BLU Cell Viability Analyzer (Beckman Coulter). To assess T cell activation, CLDN18.2$^+$ KATO III cells were plated onto a 96-well plate and incubated overnight at 37 °C. The following day, transduced CLDN18.2-TAC-expressing T cells were added to the now adherent KATO III cells and these co-cultures were incubated for 4 h at 37 °C to induce T cell activation. The reaction was stopped with the addition of 20 mM EDTA. T cells were then collected, immunostained for CD8 and CD69, and assayed by flow cytometry as described below. For TAC cell-surface expression, levels of each CLDN18.2-TAC variant was assessed by flow cytometry using an anti-Myc antibody following co-culture of TAC-expressing T cells with CLDN18.2$^+$ KATO III cells.

Flow cytometry

Flow cytometry was carried out using the ID7000 Spectral Analyzer (Sony) using the 3-color configuration (violet: 405 nm, blue: 488 nm, red: 637 nm). Spectral unmixing was performed using the ID7000 software and flow data was analyzed using FCS Express (De Novo Software). Prior to flow cytometry, T cells were stained at 4 °C using the following antibodies: 1:25 AF-488 anti-TCR α/β (#306712; Biolegend), 1:50 anti-Myc (#2276S; Cell Signaling), 1:25 APC anti-mouse IgG2a (#407109; Biolegend), 1:100 AF-700 anti-CD8a (#56-0087-42; Thermo), 1:100 BV-650 anti-CD4 (#317436; Biolegend), 1:50 Pacific Blue anti-CD69 (#310920; Biolegend). After antibody staining, cells were fixed with 4% paraformaldehyde, washed, then measured by flow cytometry.

In vivo methods

All animal work was carried out in compliance with federal laws for animal ethics, in accordance with the Canadian Council on Animal Care (CCAC). In vivo studies were performed at the McMaster University vivarium (Hamilton, Canada) with animal research ethics board (AREB; McMaster University) approval and have been reported herein in accordance with ARRIVE guidelines[47]. Adult female immune-deficient NSG (NOD.Cg-*Prkdc*^{scid}*Il2rg* ^{tm1Wjl}/SzJ; Jackson Labs) or NRG (NOD.Cg-*Rag1*^{tm1Mom}*Il2rg*^{tm1Wjl}/SzJ; Jackson Labs) mice were used for NALM6/NCI-N87 or OE19 tumor models, respectively, except for those in Fig. S2 where both male and female NRG mice were used. Mice were inoculated with either human CLDN18.2$^+$ OE19 or NCI-N87$^{CLDN18.2}$ cells via subcutaneous (s.c.) injection into the hind flank (1×10^6 cells) or with human NALM6$^{eLuc/CLDN18.2}$ cells intravenously (i.v.) via the tail vein (5×10^5 cells). Exclusion criteria included poor tumor establishment below a cutoff threshold set a priori and animals were randomized using Studylog software (San Francisco, CA). Animal-handling staff were blinded to treatment groups until study completion. Acute human T cell treatment (CLDN18.2-TAC-transduced or control non-transduced T cells) was administered via tail vein injection as a single bolus at indicated dose levels ($1.0–12.0 \times 10^6$ cells). A no-treatment control group was included for all in vivo studies. Solid tumors were monitored biweekly using caliper measurements and tumor volume (mm^3) was calculated using the formula $v = l \times w \times h$. Liquid tumor burden was assessed by bioluminescence imaging using an IVIS Spectrum In Vivo Imaging System (Perkin Elmer) after intraperitoneal (i.p.) injection of IVISbrite D-luciferin as per the manufacturer's instructions (Perkin Elmer). For tumor monitoring procedures animals were first anesthetized with inhaled isoflurane prior to assessment. Animals were euthanized via cervical dislocation under anesthesia at humane endpoints or at study termination.

Protein expression and purification

Plasmids encoding for UCHT1 scFv variants were transformed into chemically competent *E. coli* SHuffle T7 cells (NEB). Transformed cells were selected with ampicillin and grown in auto-induction media [1.6% (w/v) tryptone, 1% (w/v) yeast extract, 50 mM Na_2HPO_4, 50 mM KH_2PO_4, 25 mM $(NH_4)_2SO_4$, 0.5% (v/v) glycerol, 0.05% (w/v) glucose, 0.2% (w/v) lactose, and 2 mM $MgSO_4$][20] at 18 °C on a shaker (175 RPM) for 72 h until $OD_{600} \sim 7.0$. Cells were pelleted by centrifugation at 4000 g for 30 min at 4 °C and resuspended in Ni-NTA lysis buffer [50 mM Na_2HPO_4; pH 7.5, 500 mM NaCl, 10% (v/v) glycerol, 25 mM imidazole, and 0.1% (v/v) Triton X-100] supplemented with lysozyme. Cells were lysed by sonication, centrifuged at 35,000 g for 45 min at 4 °C, and the clarified supernatant was applied to a gravity column loaded with HisPur Ni-NTA resin (Thermo). A three-step process was used to purify UCHT1; (1) Ni^{2+} affinity purification, (2) removal of the poly-His^8 tag by overnight incubation with TEV protease at 4 °C, and (3) anion exchange chromatography over a 50–600 mM NaCl gradient [10 mM Tris; pH 7.5, 10% (v/v) glycerol] on a MonoQ 5/50 GL column (Cytiva) using an AKTA Purifier FPLC system (Cytiva). Protein samples following anion exchange were run on SDS-PAGE gels and fractions containing purified recombinant UCHT1 scFv were pooled and dialyzed overnight into phosphate buffer saline [PBS; 137 mM NaCl, 2.7 mM KCl, 10 mM Na_2HPO_4, and 1.8 mM KH_2PO_4; pH 7.4] supplemented with 10% (v/v) glycerol. Proteins were aliquoted, flash frozen in liquid nitrogen, and stored at – 80 °C. Protein concentrations were determined on a Nanodrop spectrophotometer (Thermo) at 280 nm using the ε1% value

for each variant as determined using ProtParam (ExPASy). The purity of each final UCHT1 preparation was validated by imaging Coomassie Brilliant Blue (CBB)-stained SDS-PAGE or Native-PAGE gels, or anti-Myc immunoblots loaded with either 4 µg (CBB) or 0.4 µg (anti-Myc) of each UCHT1 variant.

SDS-PAGE and immunoblotting

Protein samples were denatured in 1 × Laemmli sample buffer [63 mM Tris-HCl; pH 6.8, 10% (v/v) glycerol, 2% (w/v) SDS, 0.005% (w/v) bromophenol blue, 3.75% (v/v) 2-mercaptoethanol] at 95 °C for 10 min, then resolved on 12% SDS-PAGE gels. Gels were either CBB-stained or transferred to PVDF using a modified Fast Transfer Buffer[48] on a Trans-Blot Turbo Transfer System (Bio-Rad). For immunoblotting, PVDF membranes were blocked for 1 h at room temperature in 5% non-fat milk powder in PBS containing 0.15% (v/v) Triton X-100 (PBST), followed by incubation overnight at 4 °C with 1:1000 anti-Myc primary antibody (#2276; Cell Signaling). Probed membranes were washed with PBST, and primary antibodies were detected using 1:10,000 peroxidase-coupled anti-mouse secondary antibodies (Jackson ImmunoResearch) and SuperSignal West Pico PLUS Chemiluminescent Substrate (Thermo). Both CBB-stained gels and immunoblotted membranes were imaged on a ChemiDoc MP System (Bio-Rad).

Native-PAGE

Protein samples were mixed on-ice with 1 × non-reducing Native sample buffer [63 mM Tris–HCl; pH 6.8, 10% (v/v) glycerol, 0.005% (w/v) bromophenol blue] then resolved on 12% Native-PAGE gels without the addition of SDS in the gels or running buffer. Native-PAGE gels were either CBB-stained or transferred to PVDF as described for SDS-PAGE gels. For immunoblotting, PVDF membranes were blocked, probed with anti-Myc primary antibody, and imaged as above.

Thermal shift assay

Purified UCHT1 scFv variants were diluted to 0.5 mg/mL in PBS with 10% (v/v) glycerol, loaded into Tycho NT.6 glass capillaries (NanoTemper), and allowed to equilibrate to room temperature. Thermal melts were performed on a Tycho NT.6 system (NanoTemper) using default settings over a 35–95 °C range. Protein unfolding was tracked at 350 nm relative to folded protein at 330 nm and data were graphed. Thermal denaturation midpoint (T_m) was determined for each UCHT1 scFv variant using GraphPad Prism by fitting a sigmoidal nonlinear regression curve to the raw data and calculating the inflection point.

Size-exclusion chromatography

Purified UCHT1 variants were diluted to 0.5 mg/mL in PBS with 10% (v/v) glycerol and 300 µL of each variant was loaded independently onto a Superdex 75 Increase 10/300 GL column (Cytiva). Proteins were fractionated by running PBS at 0.5 mL/min over 1.1 column volumes (26 mL) using an AKTA Purifier FPLC system (Cytiva) at 4 °C and collected into 0.5 mL fractions. Elution of UCHT1 from the column was tracked at 280 nm, and protein samples from each fraction were run on SDS-PAGE gels that were then Coomassie-stained and imaged. Chromatographic traces were prepared in GraphPad Prism. The following protein standards were used to calibrate the Superdex 75 Increase 10/300 GL column: alcohol dehydrogenase (150 kDa), bovine serum albumin (BSA; 66 kDa), carbonic anhydrase (29 kDa), and aprotinin (6.5 kDa). Void volume was determined to be 7.81 mL using Blue Dextran. The apparent molecular weight of the purified UCHT1 scFv variants was calculated by aligning the peak elution volume for each variant onto a standard curve generated from the above calibration.

In vitro binding kinetics

Bio-layer interferometry (BLI) assays were performed on the Octet Red96 system (Sartorius). Purified UCHT1 scFvs were diluted in BLI kinetics buffer [1 × PBS with 0.1% (w/v) BSA and 0.02% (v/v) Tween-20] to create a 100–4 nM dilution series. Streptavidin-coated probes (Sartorius) were pre-wet in BLI kinetics buffer for 600 s, washed twice for 300 s, then loaded for 300 s in a 5 µg/mL solution of biotinylated CD3εδ heterodimer (#CDD-H82F6; ACROBiosystems) prepared in kinetics buffer. Probes were washed for 300 s, baselined for 30 s, then association was measured by incubation of CD3εδ-loaded probes with UCHT1 scFv variants for 300 s. Subsequently, dissociation rates were measured over a 900 s period in kinetics buffer without UCHT1. All steps were performed at 30 °C with 1000 RPM shaking. Independent replicates for each UCHT1 scFv were assayed on unique probes without regeneration. Data were analyzed using GraphPad Prism software by fitting binding curves using nonlinear regression with global analysis across multiple concentrations for each UCHT1 variant.

Statistical analysis

For in vitro, cellular functional, and in vivo experiments biological replicates were independently prepared and assayed in parallel. NALM6 and OE19 in vivo studies utilizing lower doses of TAC-engineered T cells (1.0×10^6 cells) were done in two separate experiments and data from individual mice were pooled for analysis. All data were analyzed using GraphPad Prism (10.1.0) software. Data are reported as means ± standard deviation (SD) of independent replicate experiments (n). Statistical analysis was performed as follows: Student's t-test for analysis of cellular functional assays, logrank test for in vivo survival, or Brown-Forsythe and Welch ANOVA with Dunnett's T3 post hoc test when comparing in vitro kinetic data. Statistical significance was set at $p \leq 0.05$ and test comparisons are indicated on graphs.

Data availability

All data generated and analyzed during this study are included in this published article and/or corresponding Supplementary Information files. Original data, including uncropped gels and immunoblots, are available from the corresponding authors upon request.

Received: 9 October 2024; Accepted: 23 January 2025
Published online: 25 February 2025

References

1. De Marco, R. C., Monzo, H. J. & Ojala, P. M. CAR T cell therapy: A versatile living drug. *Int. J. Mol. Sci.* **24**, 6300 (2023).
2. Albelda, S. M. CAR T cell therapy for patients with solid tumours: Key lessons to learn and unlearn. *Nat. Rev. Clin. Oncol.* **21**, 47–66 (2024).
3. Cappell, K. M. & Kochenderfer, J. N. Long-term outcomes following CAR T cell therapy: What we know so far. *Nat. Rev. Clin. Oncol.* **20**, 359–371 (2023).
4. Hamieh, M., Mansilla-Soto, J., Rivière, I. & Sadelain, M. Programming CAR T cell tumor recognition: Tuned antigen sensing and logic gating. *Cancer Discov.* **13**, 829–843 (2023).
5. Klebanoff, C. A., Chandran, S. S., Baker, B. M., Quezada, S. A. & Ribas, A. T cell receptor therapeutics: Immunological targeting of the intracellular cancer proteome. *Nat. Rev. Drug Discov.* **22**, 996–1017 (2023).
6. Burton, J. et al. Inefficient exploitation of accessory receptors reduces the sensitivity of chimeric antigen receptors. *Proc. Natl. Acad. Sci. USA* **120**, e2216352120 (2023).
7. Mansilla-Soto, J. et al. HLA-independent T cell receptors for targeting tumors with low antigen density. *Nat. Med.* **28**, 345–352 (2022).
8. Liu, Y. et al. Chimeric STAR receptors using TCR machinery mediate robust responses against solid tumors. *Sci. Transl. Med.* **13**, eabb5191 (2021).
9. Baeuerle, P. A. et al. Synthetic TRuC receptors engaging the complete T cell receptor for potent anti-tumor response. *Nat. Commun.* **10**, 2087 (2019).
10. Helsen, C. W. et al. The chimeric TAC receptor co-opts the T cell receptor yielding robust anti-tumor activity without toxicity. *Nat. Commun.* **9**, 3049 (2018).
11. Beverley, P. C. & Callard, R. E. Distinctive functional characteristics of human "T" lymphocytes defined by E rosetting or a monoclonal anti-T cell antibody. *Eur. J. Immunol.* **11**, 329–334 (1981).
12. Bezverbnaya, K. et al. T-cell engineered with a fully humanized B-cell maturation antigen-specific T-cell antigen coupler receptor effectively target multiple myeloma. *Cytotherapy* **25**, 490–501 (2023).
13. Bezverbnaya, K. et al. Development of a B-cell maturation antigen-specific T-cell antigen coupler receptor for multiple myeloma. *Cytotherapy* **23**, 820–832 (2021).
14. Olson, D.J., Dumbrava, E., Saibil, S., Gutierez, M., Iqbal, S., Sohal, D., Apostolopoulou, M., Moss, K., Adib, D. & Schlechter, B. (2023) 738 A phase 1/2 study investigating the safety and efficacy of autologous TAC T cells in subjects with unresectable, locally advanced or metastatic claudin 18.2+ solid tumors. In *Regular and Young Investigator Award Abstracts* pp. A831–A831. BMJ Publishing Group Ltd.
15. Helsen, C. W., Bramson, J., Dvorkin-Gheva, A., Denisova, G. F., Bezverbnaya, K. & Mwawasi, K. A. (2020) Patent US20200392247A1: T cell-antigen coupler with y182t mutation and methods and uses thereof., 1–20.
16. Zhu, Z. & Carter, P. Identification of heavy chain residues in a humanized anti-CD3 antibody important for efficient antigen binding and T cell activation. *J. Immunol.* **155**, 1903–1910 (1995).
17. Xu, S. X., Wang, L., Ip, P., Randhawa, R. R., Benatar, T., Prosser, S. L., Lal, P., Khan, A., Nitya-Nootan, T., Thakor, G., MacGregor, H., Hayes, D., Vucicevic, A., Mathew, P., Sengupta, S., Helsen, C. W. & Bader, A. G Preclinical development of T cells engineered to express a T cell antigen coupler (TAC) targeting solid tumors expressing Claudin 18.2. *Cancer Immunol. Res.* **13**, 35–46 (2025).
18. Ziegler, S. F., Ramsdell, F. & Alderson, M. R. The activation antigen CD69. *Stem Cells* **12**, 456–465 (1994).
19. Arnett, K. L., Harrison, S. C. & Wiley, D. C. Crystal structure of a human CD3-epsilon/delta dimer in complex with a UCHT1 single-chain antibody fragment. *Proc. Natl. Acad. Sci. USA* **101**, 16268–16273 (2004).
20. Studier, F. W. Protein production by auto-induction in high density shaking cultures. *Protein Expr. Purif.* **41**, 207–234 (2005).
21. Wörn, A. & Plückthun, A. Stability engineering of antibody single-chain Fv fragments. *J. Mol. Biol.* **305**, 989–1010 (2001).
22. Gil, D. & Schrum, A. G. Strategies to stabilize compact folding and minimize aggregation of antibody-based fragments. *Adv. Biosci. Biotechnol.* **4**, 73–84 (2013).
23. Kortt, A. A., Dolezal, O., Power, B. E. & Hudson, P. J. Dimeric and trimeric antibodies: High avidity scFvs for cancer targeting. *Biomol. Eng.* **18**, 95–108 (2001).
24. Kunert, R. & Reinhart, D. Advances in recombinant antibody manufacturing. *Appl. Microbiol. Biotechnol.* **100**, 3451–3461 (2016).
25. Zhang, J.-H., Shan, L.-L., Liang, F., Du, C.-Y. & Li, J.-J. Strategies and considerations for improving recombinant antibody production and quality in Chinese hamster ovary cells. *Front. Bioeng. Biotechnol.* **10**, 856049 (2022).
26. Miller, K. D., Weaver-Feldhaus, J., Gray, S. A., Siegel, R. W. & Feldhaus, M. J. Production, purification, and characterization of human scFv antibodies expressed in Saccharomyces cerevisiae, Pichia pastoris, and Escherichia coli. *Protein Expr. Purif.* **42**, 255–267 (2005).
27. Vallejo, L. F. & Rinas, U. Strategies for the recovery of active proteins through refolding of bacterial inclusion body proteins. *Microb. Cell Fact.* **3**, 11 (2004).
28. Ramm, K., Gehrig, P. & Plückthun, A. Removal of the conserved disulfide bridges from the scFv fragment of an antibody: Effects on folding kinetics and aggregation. *J. Mol. Biol.* **290**, 535–546 (1999).
29. Kipriyanov, S. M., Moldenhauer, G. & Little, M. High level production of soluble single chain antibodies in small-scale Escherichia coli cultures. *J. Immunol. Methods* **200**, 69–77 (1997).
30. Gaciarz, A. et al. Systematic screening of soluble expression of antibody fragments in the cytoplasm of E. coli. *Microb. Cell Fact.* **15**, 22 (2016).
31. Ajina, A. & Maher, J. Strategies to address chimeric antigen receptor tonic signaling. *Mol. Cancer Ther.* **17**, 1795–1815 (2018).
32. Harish, M. & Venkatraman, P. Evolution of biophysical tools for quantitative protein interactions and drug discovery. *Emerg. Top Life Sci.* **5**, 1–12 (2021).
33. Jug, A., Bratkovič, T. & Ilaš, J. Biolayer interferometry and its applications in drug discovery and development. *TrAC Trends Anal. Chem.* **176**, 117741 (2024).
34. Abdiche, Y., Malashock, D., Pinkerton, A. & Pons, J. Determining kinetics and affinities of protein interactions using a parallel real-time label-free biosensor, the Octet. *Anal. Biochem.* **377**, 209–217 (2008).
35. Kamat, V. & Rafique, A. Designing binding kinetic assay on the bio-layer interferometry (BLI) biosensor to characterize antibody-antigen interactions. *Anal. Biochem.* **536**, 16–31 (2017).
36. Yang, D., Singh, A., Wu, H. & Kroe-Barrett, R. Comparison of biosensor platforms in the evaluation of high affinity antibody-antigen binding kinetics. *Anal. Biochem.* **508**, 78–96 (2016).
37. Waldman, A. D., Fritz, J. M. & Lenardo, M. J. A guide to cancer immunotherapy: From T cell basic science to clinical practice. *Nat. Rev. Immunol* **20**, 651–668 (2020).
38. Mao, R., Kong, W. & He, Y. The affinity of antigen-binding domain on the antitumor efficacy of CAR T cells: Moderate is better. *Front. Immunol.* **13**, 1032403 (2022).
39. Robertson, I. B. et al. Tuning the potency and selectivity of ImmTAC molecules by affinity modulation. *Clin. Exp. Immunol.* **215**, 105–119 (2024).
40. Hoffmann, M. M. & Slansky, J. E. T-cell receptor affinity in the age of cancer immunotherapy. *Mol. Carcinog.* **59**, 862–870 (2020).

41. Stone, J. D., Chervin, A. S. & Kranz, D. M. T-cell receptor binding affinities and kinetics: Impact on T-cell activity and specificity. *Immunology* **126**, 165–176 (2009).
42. Chervin, A. S. et al. The impact of TCR-binding properties and antigen presentation format on T cell responsiveness. *J. Immunol.* **183**, 1166–1178 (2009).
43. Lever, M., Maini, P. K., van der Merwe, P. A. & Dushek, O. Phenotypic models of T cell activation. *Nat. Rev. Immunol.* **14**, 619–629 (2014).
44. Zhong, S. et al. T-cell receptor affinity and avidity defines antitumor response and autoimmunity in T-cell immunotherapy. *Proc. Natl. Acad. Sci. USA* **110**, 6973–6978 (2013).
45. Lever, M. et al. Architecture of a minimal signaling pathway explains the T-cell response to a 1 million-fold variation in antigen affinity and dose. *Proc. Natl. Acad. Sci. USA* **113**, E6630–E6638 (2016).
46. Shalaby, M. R. et al. Development of humanized bispecific antibodies reactive with cytotoxic lymphocytes and tumor cells overexpressing the HER2 protooncogene. *J. Exp. Med.* **175**, 217–225 (1992).
47. Percie du Sert, N. et al. Reporting animal research: Explanation and elaboration for the ARRIVE guidelines 20. *PLoS Biol.* **18**, e3000411 (2020).
48. Garić, D., Dumut, D. C., Centorame, A. & Radzioch, D. Western blotting with fast SDS-PAGE and semi-dry protein transfer. *Curr. Protoc.* **3**, e833 (2023).

Acknowledgements
We thank Dr. Jonathan L. Bramson and his staff at McMaster University, specifically Drs. Joanne Hammill, Craig Aarts, and Chris Baker for their technical assistance.

Author contributions
T.M.M., T.B., S.X.X., L.W., C.W.H., and W.A.H. conceptualization, methodology, investigation, data analysis; P.I. investigation, data analysis; T.N.N. and G.T. methodology; T.M.M., C.W.H., and W.A.H., manuscript writing-original draft; All authors, writing-review & editing. A.G.B., C.W.H., and W.A.H., supervision; W.A.H., funding acquisition.

Funding
T.M.M. was jointly funded by Mitacs Accelerate awards (IT23589 and IT37046) and by Triumvira Immunologics (Hamilton, Canada). This work was supported by a grant from the Canadian Institutes of Health Research Project Grant (PJT-173491) to W. A. H.

Declarations

Competing interests
This work has been funded in part by Triumvira Immunologics, a for-profit biotechnology R&D company and current developer and shared patent-holder of the TAC receptor technology (patents #US11110123B2 and #US10435453B2). Authors T.B., S.X.X., L.W., P.I., T.N.N., G.T., A.G.B., and C.W.H. were employed by Triumvira Immunologics during completion of this study. Authors T.M.M. and W.A.H. declare no financial or competing interests.

Additional information
Supplementary Information The online version contains supplementary material available at https://doi.org/10.1038/s41598-025-87944-2.

Correspondence and requests for materials should be addressed to C.W.H. or W.A.H.